

COOPERATIVE FULL WAVEFORM AND GRAVIMETRIC INVERSION

RAUL U. SILVA¹, JONAS D. DE BASABE¹, MRINAL K. SEN²,
MARIO GONZÁLEZ-ESCOBAR¹, ENRIQUE GÓMEZ-TREVIÑO¹ and
SELENE SOLORZA-CALDERÓN³

¹ *Earth Sciences Division, Centro de Investigación Científica y Educación Superior de Ensenada (CICESE), Baja California, México. jonas@cicese.mx.*

² *Institute for Geophysics, The University of Texas at Austin, TX, U.S.A.*

³ *Facultad de Ciencias, Universidad Autónoma de Baja California, Baja California, México.*

(Received October 18, 2019; revised version accepted August 9, 2020)

ABSTRACT

Silva, R.U., De Basabe, J.D., Sen, M.K., González-Escobar, M., Gómez-Treviño, E. and Solorza-Calderón, S., 2020. Cooperative full waveform and gravimetric inversion. *Journal of Seismic Exploration*, 29: 549-573.

There has been an increasing interest in recent years in the inversion of multiple geophysical data sets to obtain a consistent subsurface model for exploration and exploitation purposes. We employ cooperative inversion of gravity and seismic data for estimating a velocity and density model which fits observed data on the surface. This particular combination is motivated by the fact that the horizontal resolution of a model can be resolved by gravity inversion while the vertical resolution can be better estimated from the seismic data. We develop an iterative scheme based on full waveform inversion (FWI) and petrophysical relations that minimizes the misfit between the observed and synthetic data measured at the surface for gravimetric stations and seismograms. Our algorithm exploits the benefits of each of the geophysical methods. It uses the adjoint-state method for the computation of the gradient needed for FWI and uses a constrained Conjugate Gradient Least Squares method for gravimetric inversion subject to the discrepancies between the density and the velocity models using petrophysical relationships between these properties. We tested our algorithm on three synthetic models: The first model is a Texas-shaped structure with a high-velocity region beneath

some horizontal layers with low velocities, the second example consists of a more complex version of the Texas-shaped model adding more heterogeneities and faults with the addition of random noise on the observed data, and the final model is a 3D example of cooperative gravimetric and full waveform inversion. In all the examples, we were able to fit the data and achieve iterative convergence, recovering the interface between layers and the top and shape of the higher-velocity body. The numerical examples demonstrate that the proposed method can be used to successfully combine gravimetric and seismic data sets to obtain a consistent subsurface model without incurring the computational cost of traditional joint-inversion methods.

KEY WORDS: full waveform inversion (FWI), gravimetric inversion, finite differences.

INTRODUCTION

The challenges of geophysical exploration for the exploitation of natural resources and reservoir characterization are increasing and require incorporation of more information collected on the surface. In order to be able to obtain more detailed subsurface models, we need to be able to combine the data from different geophysical methods. In this paper, we study the acoustic properties of the subsurface layers using seismic observations and density variation through the measurement of gravity anomalies.

Full Waveform Inversion (FWI) (Tarantola, 1984; 1986) is a powerful seismic-imaging method used to estimate a velocity model (P-wave velocity model for acoustic FWI) with the objective of minimizing the discrepancies between observed and synthetic seismograms using a gradient-based optimization method. FWI has become a popular method (Virieux and Operto, 2009) and it has improved significantly throughout the years, reducing the computational cost and improving the resolution of the seismic image.

FWI consists of three main steps performed iteratively for the inversion. The first step is the forward modeling to compute the synthetic data starting from an initial model and obtain the residual subtracting the observed data. Several authors have used the Finite Difference Method (FDM) (Alford et al., 1974; Virieux, 1986) for waveform modeling, however, the Finite Element Method (FEM) (Marfurt, 1984) and the Spectral Element Method (SEM) (Komatitsch and Tromp, 1999) are becoming increasingly popular. The second step is to back-propagate the residual wave-field (adjoint field). Then, a cross-correlation between the forward and the adjoint wave-field is computed and, adding over all times and all sources, a velocity gradient is obtained. This is the well-known adjoint method (Plessix, 2006), which reduces significantly the computational cost because only two forward modelings are required in each iteration of the inversion process. On the final step, the velocity model is

updated adding to the starting model the scaled velocity gradient using a line-search method to determine the increment. If the observed and synthetic data do not match, these steps are performed iteratively until a stop criterion is reached. This methodology has provided good results for stratigraphic and predominantly horizontal layered models. Despite the good results both in acoustic and elastic media, density variation has largely been ignored (Virieux and Operto, 2009).

The study of gravimetric data is important for estimating density variations of the subsoil measuring the gravity or the gravity gradient tensor on the surface (Zhdanov et al., 2004). Several forward modeling methods exist to compute gravity anomalies by solving Poisson's equation for the gravitational potential. Among the best-known methods is the analytical solution for prismatic (Nagy, 1966; Bhattacharyya and Leu, 1977), however, solutions for other geometries are readily available (Talwani, 1965; Johnson and Litehiser, 1972; Werner, 1994; García-Abdeslem, 2005). Analogous to waveform modeling, gravity modeling has been also explored using FEM recently (Martin et al., 2017). In this work, we will use the solution for uniform rectangular prisms to be congruent with the grid used on finite differences for waveform modeling.

Gravimetric inversion for density estimation is a linear problem. This method is well known for estimating structures with horizontal changes of mass distribution. The solution is straightforward using Gauss-Newton minimization (Sen and Stoffa, 2013) to obtain a density model inverting the Hessian matrix on a single step. This method is widely used among geophysicists because of its fast convergence, however, it is computationally expensive and infeasible for large-scale problems, because a square matrix needs to be stored and inverted. One alternative for this problem is to use the Conjugate Gradient Least Squares method (CGLS). This solves the inverse problem without the need to form and store the Hessian matrix (Sen and Stoffa, 2013).

Taking into consideration the sensitivity and resolution of each method, a complex geological environment can be investigated by exploiting the advantages of both methods using a cooperative inversion scheme of seismic and gravimetric data sets. Vozoff and Jupp (1975) were the first to perform joint inversion for different geophysical data sets, namely resistivity and magnetotelluric data. Following this, numerous methodologies and different geophysical data-inversion schemes emerged becoming a popular cooperative integration technique for the reduction of non-uniqueness and ambiguity in the interpretation of the Earth model. Depending on the constraints in the optimization problem, the joint inversion schemes can be classified into petrophysical, structural or statistical. Petrophysical joint inversion is subject to empirical relationships of the model parameters (Menichetti and Guillen, 1983; Lees and VanDecar, 1991; Zeyen and Pous, 1993), structural joint inversion seeks to minimize the cross product of the

gradient of each model parameter (Gallardo and Meju, 2003, 2004) and statistical joint inversion tries to solve the problem attaching to each grid cell of the model a mean point (fuzzy c-mean) depending on the number of c-means (Paasche and Tronicke, 2007; Romero and Gallardo, 2015).

One of the most examined joint geophysical interpretation is the cooperative inversion of seismic and gravimetric data since this method complements each other and both theories depend on the density of the medium. One such example is the work of Roy et al. (2005) which performs first-arrival travel time inversion jointly with gravity data using very fast simulated annealing. Works using seismic and gravity data were presented later (Tondi et al., 2009; Lin et al., 2012; Lin and Zhdanov, 2017; Colombo and Rovetta, 2018). On the other hand, Blom et al. (2017) stress the importance of density in geological processes and present a study for the role of density using seismic and gravimetric data, concluding that density estimation requires a strong a priori model to be able to determine it as an independent parameter.

We propose a novel cooperative inversion scheme using gravimetric inversion, a petrophysical relation and FWI. Petrophysical relationships between P-wave and density were presented first by Gardner et al. (1974), but lately Brocher (2005) documented a data compilation of crustal rocks from which he computed a polynomial fit, comparing it with other empirical relationships. We perform a gravimetric inversion constraining the density model obtained using Gardner's equation from the velocity model provided after FWI. Such constraint will be strong enough to avoid shallower models due to the nature of the gravimetric potential method. We use again a petrophysical relation to convert the density model into a velocity model and apply one iteration of FWI to obtain a new velocity model that better fits the seismic data. This process is performed iteratively until FWI converges to a solution, ensuring a data fit in seismic and gravity data. The importance of performing these steps sequentially is that it is more robust than trying to invert for velocity and density jointly, it has a lower computational cost and it allows for a better control of each problem separately.

Using this scheme, we obtain complex geological models that include a stratigraphic part around a body of high density-velocity. The gravimetric inversion can detect the higher density structure while FWI recovers the horizontal folded layers, including the top of the body. The cooperative inversion combines both methods to obtain a more reasonable model that minimizes the data residual for seismic and gravity data. We perform this inversion on two synthetic 2D models and one 3D model and observe that the results have less artifacts than those obtained using only FWI with minimal increase in the computational cost.

FULL WAVEFORM INVERSION

The time domain wave equation (Cohen, 2002) for an acoustic medium is given by

$$\frac{1}{V^2} \frac{\partial^2 P(\mathbf{x}, t)}{\partial t^2} - \nabla^2 P(\mathbf{x}, t) = f(\mathbf{x}, t), \quad (1)$$

where P is the pressure, f is the seismic source and V the P-wave velocity of the medium, this will be the model parameter estimated in FWI. For the forward modeling problem, eq. (1) can be represented in terms of finite-differences discrete operators of the time and spatial derivatives in a time stepping loop (Alford et al., 1974).

For acoustic FWI, the least-squares functional to minimize the misfit between the observed and the synthetic pressure is given by

$$Q(V) = \frac{1}{2} \sum_{r,s} \int_0^T \|\mathbf{P}_{r,s}^{\text{obs}} - \mathbf{P}_{r,s}^{\text{cal}}\|^2 dt, \quad (2)$$

where $\mathbf{P}_{r,s}^{\text{obs}}$ is the observed pressure and $\mathbf{P}_{r,s}^{\text{cal}}$ is the synthetic pressure computed by numerically solving eq. (1). T is the total recording time, r denotes the receiver index and s the source index. This misfit functional is minimized using an iterative procedure based on computing a velocity gradient using the adjoint method for acoustic media (Plessix, 2006) given by

$$\delta = \frac{2}{V^3} \sum_s \int_0^T P^\dagger(\mathbf{x}, T-t) \frac{\partial^2 P(\mathbf{x}, t)}{\partial t^2} dt, \quad (3)$$

where P^\dagger is the adjoint pressure and also satisfies equation 1 using as source the data residual back-propagated in time. For example, for a single source

$$\begin{aligned} \frac{1}{V^2} \frac{\partial^2 P^\dagger(\mathbf{x}, T-t)}{\partial t^2} - \nabla^2 P^\dagger(\mathbf{x}, T-t) \\ = \sum_r \|\mathbf{P}_r^{\text{obs}} - \mathbf{P}_r^{\text{cal}}\| \delta(\mathbf{x} - \mathbf{x}_r). \end{aligned} \quad (4)$$

The velocity model (V) can be updated iteratively using the gradient as follows

$$V_{n+1} = V_n + \alpha_n \delta, \quad (5)$$

where α_n is the optimal step for the n -th iteration calculated using a line-search along the gradient using three or more points (Vigh and Starr, 2008). Notice that a large number of points can be used in the line-search to determine α_n , however, each additional point involves an additional forward modeling to compute eq. (2), it is therefore preferred to use a few test steps.

GRAVIMETRIC INVERSION

Newton's law of gravitation provides the gravitational potential Φ at an observation point \mathbf{x} due to a body on Earth with density distribution ρ as (Blakely, 1996)

$$\Phi(\mathbf{x}) = \int_{\Omega} \gamma \frac{\rho(\mathbf{x}')}{\|\mathbf{x} - \mathbf{x}'\|} d\mathbf{x}', \quad (6)$$

where γ is the universal constant of gravitation and \mathbf{x}' is the position for each differential element of density over the domain Ω . In this work, we will use only the vertical component of the gravity acceleration on Cartesian coordinates, given by

$$g_z(\mathbf{x}) = -\frac{\partial\Phi(\mathbf{x})}{\partial z} = -\int_{\Omega} \gamma \frac{\rho(\mathbf{x}')(z - z')}{\|\mathbf{x} - \mathbf{x}'\|^3} d\mathbf{x}'. \quad (7)$$

For the case of a rectangular prism of constant density (Banerjee and Das Gupta, 1977), the analytic solution of eq. (7) is given by

$$g_z = \left\{ \gamma \left[z \tan^{-1} \left(\frac{xy}{z|\Delta r|} \right) - x \ln(y + |\Delta r|) \right. \right. \\ \left. \left. - y \ln(x + |\Delta r|) \right] \left| \left| \begin{array}{l} \Delta x'_2 \\ \Delta x'_1 \end{array} \right| \left| \begin{array}{l} \Delta y'_2 \\ \Delta y'_1 \end{array} \right| \left| \begin{array}{l} \Delta z'_2 \\ \Delta z'_1 \end{array} \right| \right\} \rho, \quad (8)$$

where $|\Delta r| = \sqrt{x^2 + y^2 + z^2}$, $\Delta x'_k = x - x'_k$, $\Delta y'_k = y - y'_k$ and $\Delta z'_k = z - z'_k$ with $k = 1, 2$ for the prime coordinates (corners of the prism). This expression can be reduced easily for 2D media setting the y -coordinate equal to zero. Considering the contribution at stations from a model of $M = n_x \times n_z$ prism, this expression can be represented in a matrix form as

$$\mathbf{g}_z^{\text{cal}} = \mathbf{A}_g \mathbf{m}_\rho, \quad (9)$$

where $\mathbf{g}_z^{\text{cal}}$ is a $N_s \times 1$ vector the gravity anomaly, \mathbf{m}_ρ is a $M \times 1$ vector containing the density distribution and \mathbf{A}_g is a $N_s \times M$ matrix containing the part within brackets in eq. (8) as the density kernel.

The objective function for density estimation due to measurements of the vertical component of the acceleration ($\mathbf{g}_z^{\text{obs}}$) using the L-2 norm is given by

$$Q(\mathbf{m}_\rho) = \sum_{i=1}^{N_s} \left\| \frac{\mathbf{g}_{z_i}^{\text{obs}} - \mathbf{g}_{z_i}^{\text{cal}}}{\sigma_{g_z}} \right\|^2 + \alpha_{\text{reg}}^2 \|\mathbf{D}\mathbf{m}_\rho\|^2, \quad (10)$$

where α_{reg} is the regularization parameter, \mathbf{D} is the discrete operator for the gradient and σ_{g_z} is the standard deviation of the data. Solving this least-squares problem using Gauss-Newton method (Sen and Stoffa, 2013) an estimated model \mathbf{m}_ρ can be obtained as

$$\mathbf{m}_\rho = [\mathbf{A}_g^T \mathbf{C}_{dd}^{-1} \mathbf{A}_g + \alpha_{\text{reg}}^2 \mathbf{D}^T \mathbf{D}]^{-1} \mathbf{A}_g^T \mathbf{C}_{dd}^{-1} \mathbf{g}_z^{\text{obs}}, \quad (11)$$

where \mathbf{C}_{dd}^{-1} is the diagonal covariance matrix. This least-squares implementation requires to store and invert the square matrix in eq. (11) with dimensions depending on the discretization of the model, i.e., $M \times M$. For a very fine discretization we encounter storage problems due to this implementation, whereas we need a fine discretization in the model to achieve a good resolution for the seismic inversion and therefore the joint inversion. One solution for this problem is the use of the Conjugate Gradient Least Squares (CGLS) method. This method minimizes the objective function of eq. (10) without the need to form and store the square matrix from eq. (11) (Sen and Stoffa, 2013) using a typical conjugate gradient technique. This method requires as an input \mathbf{G} and \mathbf{d}^{CG} to find a solution, in this case, the density model (\mathbf{m}_ρ) for $\mathbf{G}\mathbf{m}_\rho = \mathbf{d}^{CG}$, these matrices are given by

$$\mathbf{G} = \begin{bmatrix} \mathbf{C}_{dd}^{-1/2} \mathbf{A}_g \\ \alpha_{\text{reg}} \mathbf{D} \end{bmatrix}, \quad (12)$$

$$\mathbf{d}^{CG} = \begin{bmatrix} \mathbf{C}_{dd}^{-1/2} \mathbf{g}_z^{\text{obs}} \\ \mathbf{0} \end{bmatrix}, \quad (13)$$

in this case, the matrix \mathbf{G} will be large and sparse due to the discrete operator of the Tikhonov regularization.

COOPERATIVE INVERSION

In this work we propose a sequential approach in which we solve at different stages for the densities and velocities, the resulting system is therefore more manageable and there is more control over the parameters at each stage. We call this a cooperative strategy to distinguish it from the joint strategies that solve for all the geophysical parameters together at every iteration. Unlike conventional joint inversions, where the problem is to minimize a two-part objective function (seismic and gravity errors), this cooperative inversion is based on alternately minimizing the errors in seismic and gravity data in an iterative fashion. The main reasons to perform these sequentially are to increase robustness and reduce the computational cost. Furthermore, in the proposed scheme we do not need to impose depth-dependent weights or constraints to the gravimetric inversion to avoid shallower models, this is achieved instead by using the velocity model after FWI as the *a priori* gravimetric model.

The cooperative inversion for gravity and seismic data comprises an iterative scheme shown in the diagram of Fig. 1. It involves the following steps: from a starting velocity model, we perform FWI to update the velocity model, then, using Gardner's density-velocity relationship, we perform constrained gravimetric inversion to update the density model, finally, using Gardner's velocity-density relationship, a velocity model is obtained for use in FWI. These steps are repeated until a convergence criterion is satisfied.

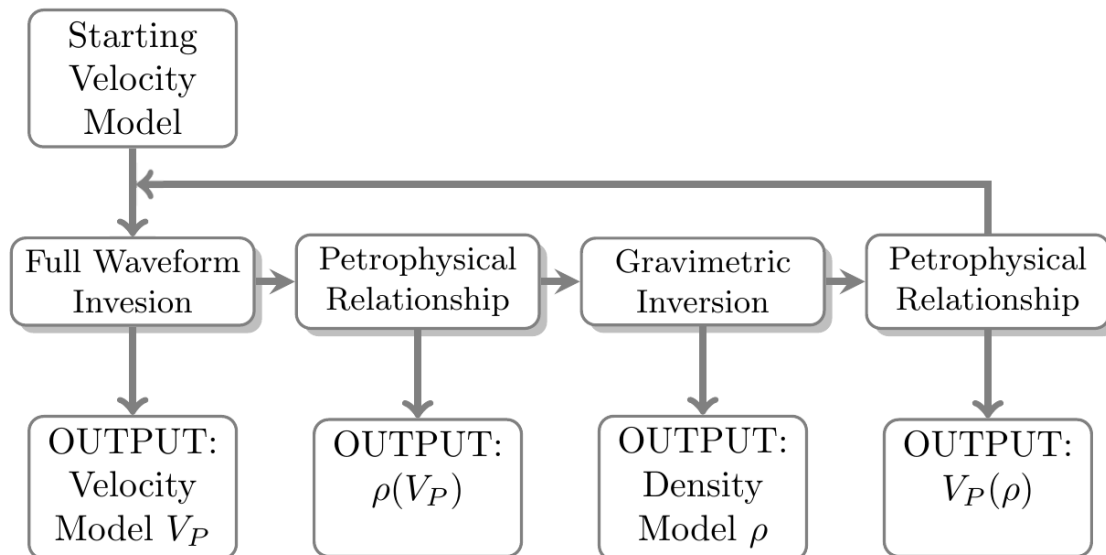


Fig. 1. Visual representation of our iterative inversion scheme for gravity and seismic data.

For the gravimetric-inversion step, we modify eq. (10) to include the velocity model obtained from FWI as a constraint as follows

$$Q(\mathbf{m}_\rho) = \sum_{i=1}^{N_s} \left\| \frac{\mathbf{g}_{z_i}^{\text{obs}} - \mathbf{g}_{z_i}^{\text{cal}}}{\sigma_{g_{z_i}}} \right\|^2 + \alpha_{\text{reg}}^2 \|\mathbf{D}\mathbf{m}_\rho\|^2 + \beta^2 \|\mathbf{m}_\rho - \mathbf{m}_{\rho(V)}\|^2, \quad (14)$$

where \mathbf{m}_ρ is the density model and $\mathbf{m}_{\rho(V)}$ is the density model obtained using a petrophysical relationship as a function of the velocity model. Notice that the third term constraints the model to be similar to the one obtained from FWI and is weighted by the parameter β ; this term allows us to restrict the gravimetric inversion and avoid shallow unrealistic models. We use the following relationship from (Gardner et al., 1974) as the petrophysical relation

$$\rho(V) = \rho_0 V_p^{k_0}, \quad (15)$$

where $\rho_0 = 0.31 \text{ g/cm}^3$ and $k_0 = 1/4$. This relationship between P-wave velocity and density is valid for velocities in the range $1.5 < V_p < 7.5 \text{ km/s}$ for most sedimentary rocks (Gardner et al., 1974); however, any other relation can be used here to accommodate a particular target model. Given the range of velocities, it is important to point out that this relationship does not apply for salt body structures in the range $4.3 < V_p < 5.0 \text{ km/s}$ for velocity and $2 < \rho < 2.2 \text{ g/cm}^3$ for density (Sheriff and Geldart, 1995).

As described in the previous section, eq. (14) can be minimized efficiently using CGLS, modifying \mathbf{G} and \mathbf{d}^{CG} from eqs. (12) and (13) as follows

$$\mathbf{G} = \begin{bmatrix} \mathbf{C}_{dd}^{-1/2} \mathbf{A}_g \\ \alpha_{\text{reg}} \mathbf{D} \\ \beta \mathbf{I} \end{bmatrix}, \quad (16)$$

$$\mathbf{d}^{CG} = \begin{bmatrix} \mathbf{C}_{dd}^{-1/2} \mathbf{g}_z^{\text{obs}} \\ \mathbf{0} \\ \beta \mathbf{m}_{\rho(V_p)} \end{bmatrix}, \quad (17)$$

where \mathbf{I} is the identity matrix. The algorithm to solve the system $\mathbf{G}\mathbf{m}_\rho = \mathbf{d}^{CG}$ is presented in algorithm 1 (Sen and Stoffa, 2013). Notice that an efficient implementation of this algorithm requires that all the matrices be stored in a sparse representation.

Algorithm 1: CGLS algorithm to iteratively solve the problem $\mathbf{G}\mathbf{m}_\rho = \mathbf{d}^{CG}$

Data:

$\mathbf{m}_0, \mathbf{d}_0 = \mathbf{d}^{CG}, \mathbf{r}_0 = \mathbf{G}^T \mathbf{d}^{CG}, \mathbf{p}_0 = \mathbf{r}_0, \mathbf{t}_0 = \mathbf{A}\mathbf{p}_0, n$ -iterations

Result: model \mathbf{m}_k

```

1  while  $k < n$  or stop criteria is satisfied do
2  |    $\alpha_k = \|\mathbf{r}_{k-1}\|^2 / \|\mathbf{t}_{k-1}\|^2$ 
3  |    $\mathbf{m}_k = \mathbf{m}_{k-1} + \alpha_k \mathbf{p}_{k-1}$ 
4  |    $\mathbf{d}_k = \mathbf{d}_{k-1} - \alpha_k \mathbf{t}_{k-1}$ 
5  |    $\mathbf{r}_k = \mathbf{G}^T \mathbf{d}_k$ 
6  |    $\beta_k = \|\mathbf{r}_k\|^2 / \|\mathbf{r}_{k-1}\|^2$ 
7  |    $\mathbf{p}_k = \mathbf{r}_k + \beta_k \mathbf{p}_{k-1}$ 
8  |    $\mathbf{t}_k = \mathbf{G}\mathbf{p}_k$ 
9  |    $k \leftarrow k + 1$ 
10 end

```

The resulting density model will give feedback to FWI using Gardner's density-velocity relationship to obtain a velocity model which will be the starting model to solve the next iteration of FWI. In practice, including the gravimetric data in the inversion process yields smoother models with less artifacts.

CONVENTIONAL JOINT INVERSION

In a conventional joint-inversion scheme, different geophysical forward problems are simultaneously solved to obtain a consistent Earth-property model which match the respective data sets measured at the surface. Usually the strategy consists of combining all the parameters into one objective function, leading to a large system of often disparate parameters (Roy et al., 2005).

Let us consider two arbitrary geophysical data sets $\mathbf{d}_m^{\text{obs}}$ and $\mathbf{d}_n^{\text{obs}}$ for the models \mathbf{m} and \mathbf{n} . The generalized objective function involving two geophysical methods is given by

$$\begin{aligned}
 Q_{\text{Total}}(\mathbf{m}, \mathbf{n}) &= \|\mathbf{d}_m^{\text{obs}} - \mathbf{d}_m^{\text{cal}}\|^2 + \alpha_m^2 \|\mathbf{D}\mathbf{m}\|^2 + \beta_m^2 \|\mathbf{m} - \mathbf{m}_{\text{apr}}\|^2 \\
 &= \|\mathbf{d}_n^{\text{obs}} - \mathbf{d}_n^{\text{cal}}\|^2 + \alpha_n^2 \|\mathbf{D}\mathbf{n}\|^2 + \beta_n^2 \|\mathbf{n} - \mathbf{n}_{\text{apr}}\|^2 \\
 &+ \gamma^2 Q_{\text{Joint}}(\mathbf{m}, \mathbf{n}) \quad ,
 \end{aligned} \tag{18}$$

where α_m and α_n are the Tikhonov regularization parameters, β_m and β_n are the *a-priori* model parameters, $\mathbf{d}_m^{\text{cal}}$ and $\mathbf{d}_n^{\text{cal}}$ are the synthetic data and $Q_{\text{Joint}}(\mathbf{m}, \mathbf{n})$ is the joint inversion constraint between both models with its respective weight γ .

There are mainly three types of joint inversion techniques, depending on the functional Q_{Joint} :

- Petrophysical joint inversion, where the models are constrained by an empirical relationship (Roy et al., 2005; Lin and Zhdanov, 2017; Blom et al., 2017), in this case $Q_{\text{Joint}}(\mathbf{m}, \mathbf{n}) = \|\mathbf{m} - \mathbf{H}(\mathbf{n})\|^2$, where \mathbf{H} is the petrophysical relation;
- Structural joint inversion (Gallardo and Meju, 2003, 2004), where the functional is used to match the structure for both models through the cross gradient, $Q_{\text{Joint}}(\mathbf{m}, \mathbf{n}) = \|\nabla \mathbf{m} \times \nabla \mathbf{n}\|^2$; and
- Statistical joint inversion, e.g., using the fuzzy c -means technique (Paasche and Tronicke, 2007; Romero and Gallardo, 2015).

We will focus on the petrophysical joint inversion. Structural and statistical joint inversion techniques are beyond the scope of this paper and will be explored in future work.

In order to compare conventional joint inversion with the cooperative inversion proposed in this work, let us minimize eq. (18) subject to an arbitrary petrophysical relationship $\mathbf{m} = \mathbf{H}(\mathbf{n})$. Using a Gauss-Newton optimization we obtain the following system

$$\begin{aligned}
 & \begin{bmatrix} \mathbf{A}_m^T \mathbf{A}_m + \alpha_m^2 \mathbf{D}^T \mathbf{D} + \beta_m^2 \mathbf{I} + \gamma^2 \mathbf{I} & -\Theta \gamma^2 \\ -\Theta \gamma^2 & \mathbf{A}_n^T \mathbf{A}_n + \alpha_n^2 \mathbf{D}^T \mathbf{D} + \beta_n^2 \mathbf{I} + \Theta^2 \gamma^2 \end{bmatrix} \begin{bmatrix} \mathbf{m} \\ \mathbf{n} \end{bmatrix} \\
 = & \begin{bmatrix} \gamma^2 [\mathbf{H}(\mathbf{n}_0) - \Theta \mathbf{n}_0] + \beta_m^2 \mathbf{m}_{\text{apr}} + \mathbf{A}_m^T [\mathbf{d}_m^{\text{obs}} - \mathbf{d}_m^{\text{cal}}(\mathbf{m}_0) + \mathbf{A}_m \mathbf{m}_0] \\ -\Theta \gamma^2 [\mathbf{H}(\mathbf{n}_0) - \Theta \mathbf{n}_0] + \beta_n^2 \mathbf{n}_{\text{apr}} + \mathbf{A}_n^T [\mathbf{d}_n^{\text{obs}} - \mathbf{d}_n^{\text{cal}}(\mathbf{n}_0) + \mathbf{A}_n \mathbf{n}_0] \end{bmatrix}, \quad (19)
 \end{aligned}$$

where \mathbf{A}_m and \mathbf{A}_n are the Fréchet derivatives for each method \mathbf{D} is the discrete operator for the gradient ∇ , \mathbf{m}_0 and \mathbf{n}_0 are the starting models (obtained from the linearized problem) and $\Theta = \frac{\partial \mathbf{H}}{\partial \mathbf{n}}$ is the derivative of the petrophysical relationship evaluated at the starting model \mathbf{n}_0 . Notice that if γ , eq. (19) is reduced to

$$\begin{aligned}
 & \begin{bmatrix} \mathbf{A}_m^T \mathbf{A}_m + \alpha_m^2 \mathbf{D}^T \mathbf{D} + \beta_m^2 \mathbf{I} & \mathbf{0} \\ \mathbf{0} & \mathbf{A}_n^T \mathbf{A}_n + \alpha_n^2 \mathbf{D}^T \mathbf{D} + \beta_n^2 \mathbf{I} \end{bmatrix} \begin{bmatrix} \mathbf{m} \\ \mathbf{n} \end{bmatrix} \\
 = & \begin{bmatrix} \beta_m^2 \mathbf{m}_{\text{apr}} + \mathbf{A}_m^T [\mathbf{d}_m^{\text{obs}} - \mathbf{d}_m^{\text{cal}}(\mathbf{m}_0) + \mathbf{A}_m \mathbf{m}_0] \\ \beta_n^2 \mathbf{n}_{\text{apr}} + \mathbf{A}_n^T [\mathbf{d}_n^{\text{obs}} - \mathbf{d}_n^{\text{cal}}(\mathbf{n}_0) + \mathbf{A}_n \mathbf{n}_0] \end{bmatrix}, \quad (20)
 \end{aligned}$$

which corresponds to the separated inversion of each data set, since there is no constraint in the objective function, and the inverse of the matrix can be

obtained by blocks. For this work we consider that \mathbf{m} is the seismic model and \mathbf{n} is the gravimetric model. The Fréchet derivatives of the seismic functional are given by $A_m(i, j) = \frac{\partial P_i}{\partial m_{V_j}}$, which correspond to the i -th derivative for the data P_i for the j -th model parameter m_{V_j} . Notice that this results in large computational cost given that it implies performing forward modelings for each grid cell of the model, as opposed to the two forward modellings required by the adjoint method for FWI. For the gravimetric inversion, $\mathbf{A}_n = \mathbf{A}_g$, where \mathbf{A}_g is given in eq. (9). Finally, for the joint inversion, the derivative of the petrophysical function is given by

$$\Theta = 4 \left(\frac{1}{0.31} \right)^4 m_\rho^3 \Big|_{m_\rho = m_{\rho 0}} \quad (21)$$

which corresponds to the derivative of Gardner's equation with respect to the density.

RESULTS

In order to test the proposed cooperative inversion algorithm and show its advantages, we apply this method to three synthetic examples. The first example is a simple layered model with Texas-shaped structure of high velocity. In the second example we add random noise to the data and demonstrate that the method can recover the model under this conditions. Finally, we apply the method to a synthetic dataset for a 3D subsurface model.

Texas-shape model I

For this example, we created a laterally heterogeneous layered model. Beneath the low velocity layers, we place a structure with the shape of Texas, as shown in Fig. 2a. The shallow layers have lower velocities (between 1500 and 2000 m/s) with respect to the deepest layer (≈ 3400 m/s). In addition to the high-velocity body, we placed two targets at medium depth to the left and to the right of the body. We used Gardner's density-velocity relationship to obtain the density model for gravity data as shown in Fig. 2c. Notice that the velocity values of the model are within the range of applicability of Gardner's equations.

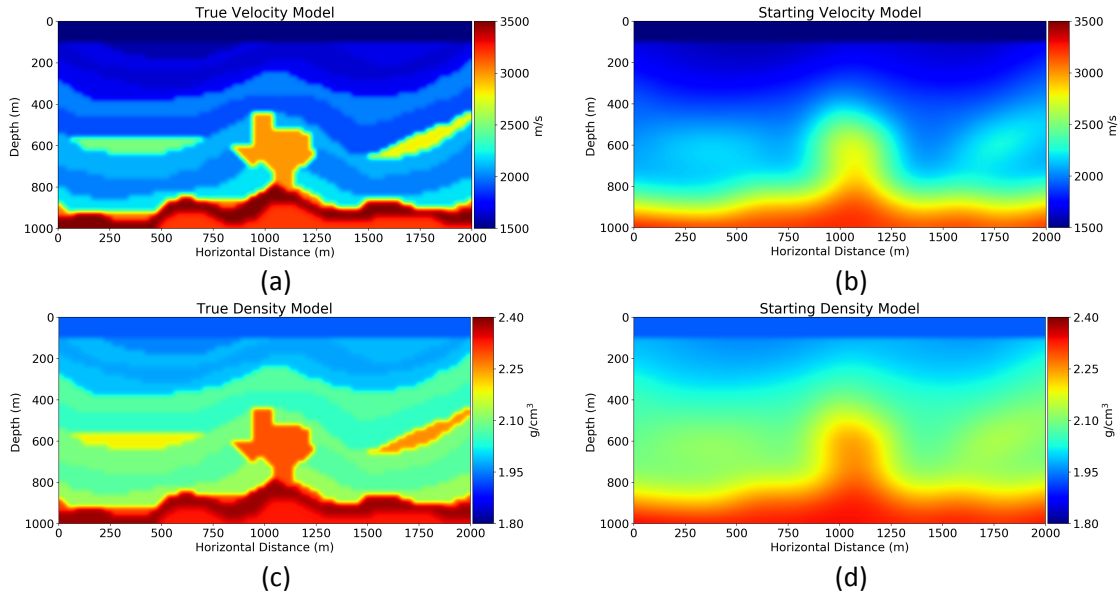


Fig. 2. Texas-shaped true velocity model I (a) and its smoothing set as a starting model (b). Texas-shaped true density model I (c) and the starting density model (d). These models are obtained using Gardner density-velocity relationship.

The synthetic geophysical model covers a horizontal distance of 2000 m and a depth of 1000 m for both seismic and gravimetric data. In order to be able to compare the cooperative and joint inversion strategies, we use a smaller mesh for this model ($n_x = 100, n_z = 50$). We modeled $n_s = 10$ sources equally spaced along the surface and recorded at $n_r = 100$ receivers along the surface for the seismic and gravimetric stations. The total record time for the seismograms is 2 seconds and the time sampling depends on the stability condition of the forward modeling, resulting in $n_t = 750$ samples. The source time function is a Ricker wavelet with a peak frequency of 8 Hz. In summary, we have $n_t \times n_r \times n_s = 750\,000$ seismic data points and $n_r = 100$ gravimetric data points, and are computing a model of $n_x \times n_z = 5\,000$ cells for this simple example, therefore, the seismic problem is over-determined whereas the gravimetric problem is under-determined. In this case, the number of seismograms and gravimetric stations are equal. We emphasize that the method does not require that the number of stations be the same, however, we use the same location for the receivers for simplicity. Often in practice the number of gravimetric stations are less than the seismic stations, the method can accommodate for this but the reduction in computational cost would be negligible.

For comparison purposes, we use the same parameters and starting models in all the methods and perform 50 iterations. Furthermore, we also include the results of the separate inversions for seismic (FWI using adjoint method) and gravity (CGLS unconstrained). For the particular case of the

conventional joint inversion, the parameter γ was chosen empirically in a similar way as in the L-curve method (Hansen, 1992).

First, let us compare the results for the velocity model (Fig. 3). The conventional FWI process recovers the stratigraphic information including the medium-depth targets, as shown in Fig. 3a. The shape and velocity values of the high-contrast body are also approximately recovered. This result is similar to the one obtained using the proposed cooperative inversion (Fig. 3c). For the conventional joint inversion process (Fig. 3e), the general geometry is recovered, however, the basement, the Texas-shape body and the medium-depth targets have lower velocities and lower resolution. Fig. 4 shows the normalized seismic misfits of the three methods with respect to the iteration number. The joint-inversion scheme stagnates after the 10th iteration, but FWI and the cooperative scheme achieve a smaller misfit.

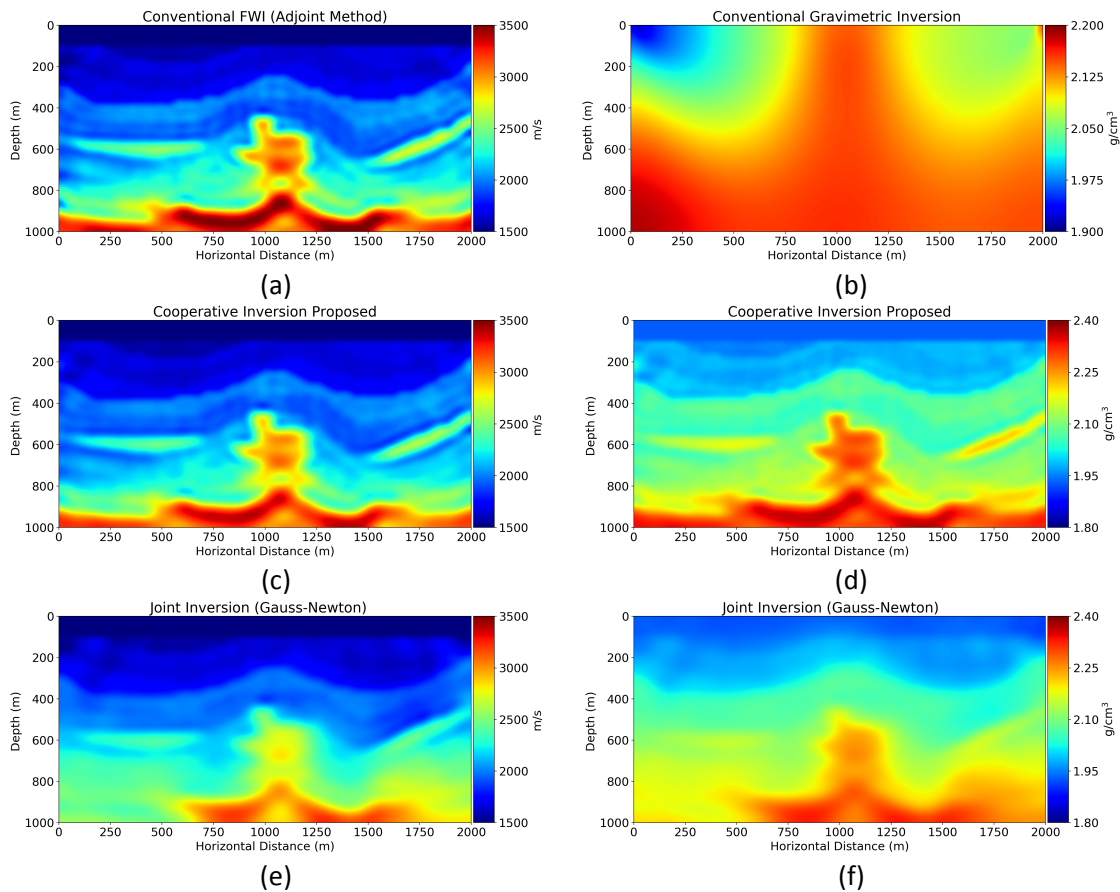


Fig. 3. Texas-shape velocity model I results for (a) conventional FWI using adjoint method, (c) petrophysical cooperative inversion, and (e) conventional joint inversion using Gauss-Newton. Texas-shaped density model I results for (b) conventional gravimetric inversion, (d) petrophysical cooperative inversion and (f) conventional joint inversion using Gauss-Newton.

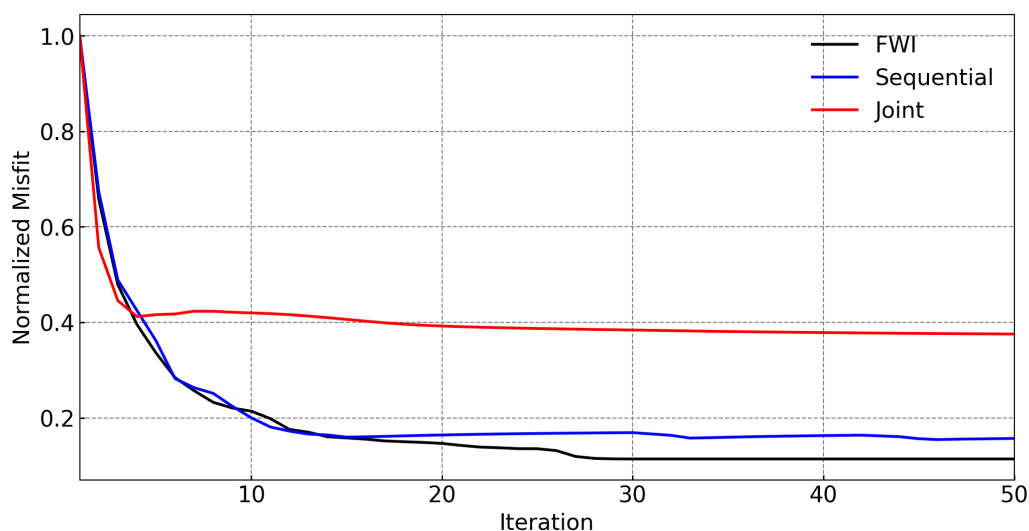


Fig. 4. Normalized misfit for seismic (red) and gravity (blue) for the Texas-shaped model I.

The results of the computed densities are shown in Fig. 3. Once again, the model loses the stratigraphic information when conventional gravimetric inversion is employed (Fig. 3b), resulting on a shallower density model. When conventional joint inversion is applied, the shape and position of the central body is obtained, however, the two targets at the left and right of the model are not identified (Fig. 3f). On the other hand, using cooperative inversion (Fig. 3d), all the targets are recovered better than with the other two methods.

Table1. Cost of the objective function and computational cost for 50 iterations for each inversions method discussed. The computational cost is normalized with respect to the cost of conventional FWI.

| Inversion Method | Objective Function Cost Reduction | Computational Time (50 Iterations) |
|--------------------|-----------------------------------|------------------------------------|
| Conventional Joint | 37.5 % | 681.63 |
| Conventional FWI | 11.4 % | 1.00 |
| Cooperative | 15.6 % | 1.02 |

The main difference between the three methods is in the computational cost. Table 1 shows the execution times for performing 50 iterations with each of the 3 methods, normalized using the time of the conventional FWI. The computational cost for conventional joint inversion using the Gauss-Newton method is significantly higher than that of the other methods, this is mainly due to the computation of the Fréchet derivatives. On the other hand, the overhead of the proposed cooperative scheme is comparatively small, amounting to 2 % in this example, and the computational cost of inverting the gravimetric data is almost negligible (0.3 % of the cost of FWI).

Texas-shape model II with noisy data

For this example, we modify the Texas-shaped model I from the previous example by increasing its complexity and resolution ($n_x = 200, n_z = 100$). We added more heterogeneities to the low-velocity layers and added faults in some layers of the model, keeping the Texas-shaped body (see Fig. 5a). Additionally, we put five objects at different depths with an appreciable velocity contrast, these objects emulate geological traps. We discretize the synthetic geophysical model covering a horizontal distance of 2000 m and a depth of 1000 m for both seismic and gravimetric data. In this example, we modeled 100 sources equally spaced along the surface and recorded at 200 receivers along the surface for synthetic seismometers and gravimetric stations. The total record time for the seismograms is 2 s and the time sampling depends on the stability condition of the forward modeling. The source time function is a Ricker wavelet with a peak frequency of 15 Hz. Furthermore, we add Gaussian random noise of 5 % of the standard deviation to the seismic and gravimetric data.

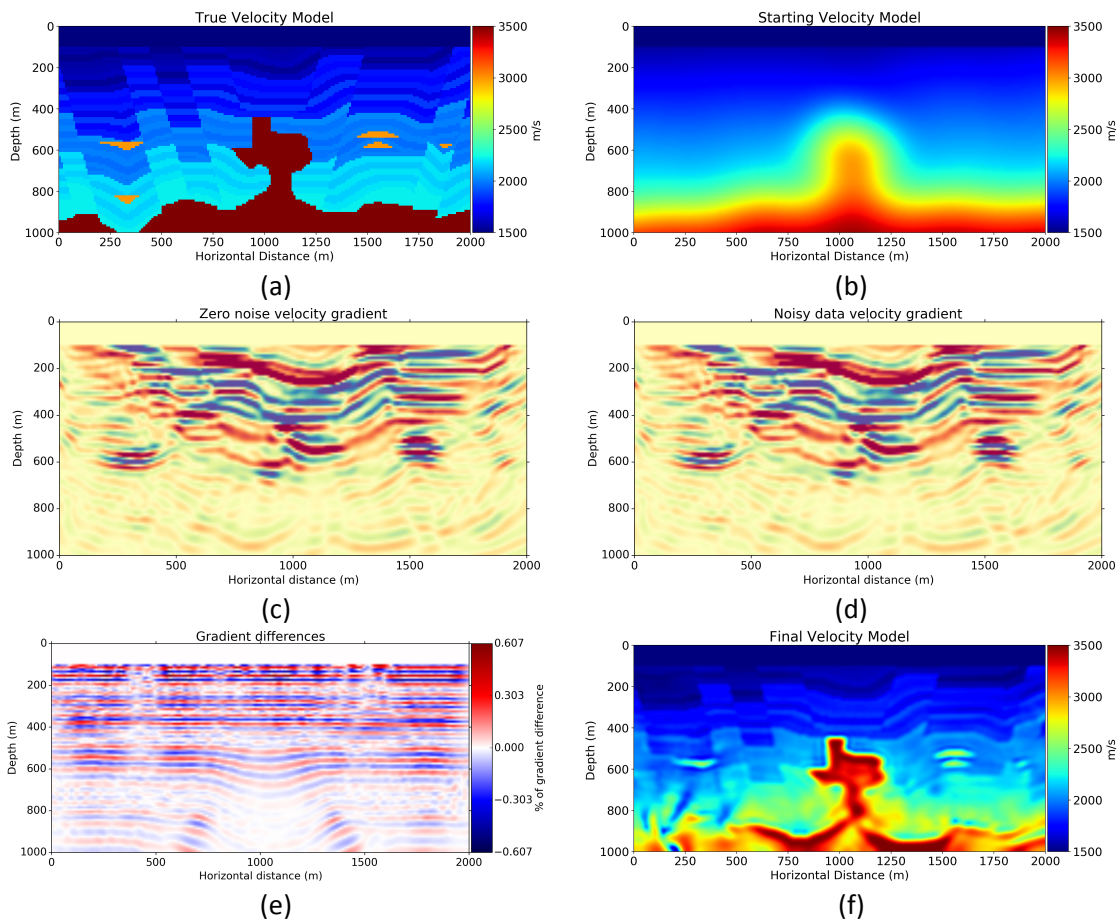


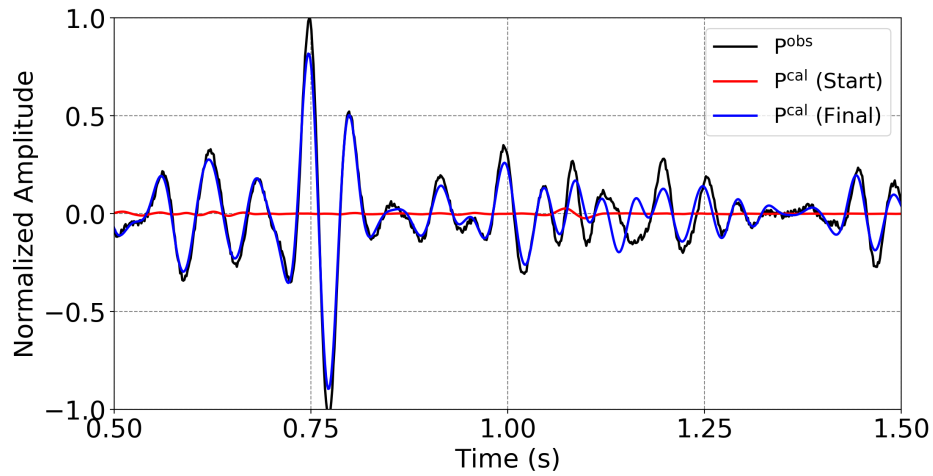
Fig. 5. Texas-shaped velocity model II (a) and starting model (b). Velocity gradients using noise-free data (c) and with 5 % of noise (d). The difference in percentage is shown in (e). Both gradients are muted where the water layer is located. Texas-shaped velocity model II results using cooperative inversion with noise in the data (f).

In order to measure the effect of random noise on the inversion procedure, we show in Fig. 5 the velocity gradients for clean and noisy data, as well as the difference. Comparing Figs. 5c and 5d, we conclude that the gradient is not significantly affected by the noise. Indeed, the difference between the gradients with and without noise is smaller than 0.6%, as shown in Fig. 5e. The results after 300 iterations are shown in Fig. 5f. Comparing with the true velocity model, we observe that the shape of the high-velocity body is recovered as well as some structural information on the layers: the faults are detected properly and the layers with their respective velocity values. The geologic traps are recovered by the algorithm, except the one closest to the basement.

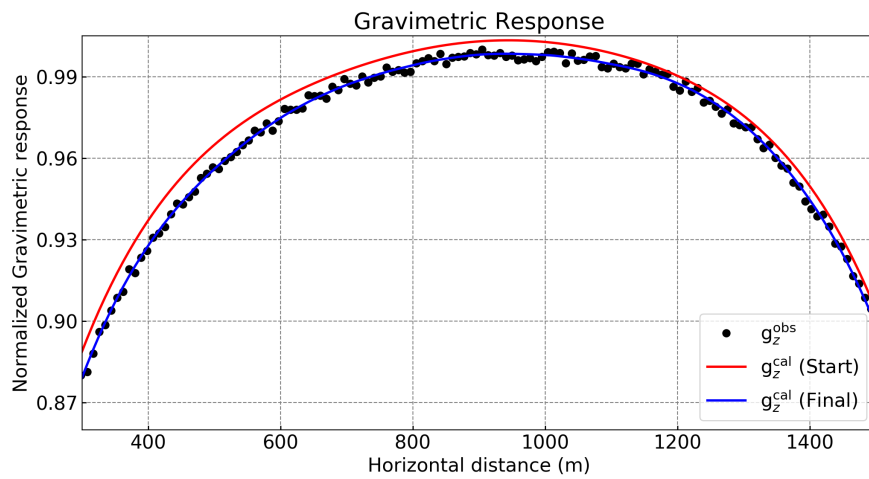
In Fig. 6a we show the observed seismograms with noise from one of the stations together with the synthetic seismograms computed from the starting and final models. The seismogram computed from the final model shows a good match to the observed data in phase and amplitude, except between 1.1 and 1.2 s. We display in Fig. 6b the gravimetric data with noise between 300 and 1500 m, together with the anomaly computed from the initial and final models, showing a very good fit. The misfit convergence (Fig. 6c) shows that the seismic and gravimetric inversions converge monotonically, with the gravimetric part showing a faster convergence.

Texas-shape 3D model

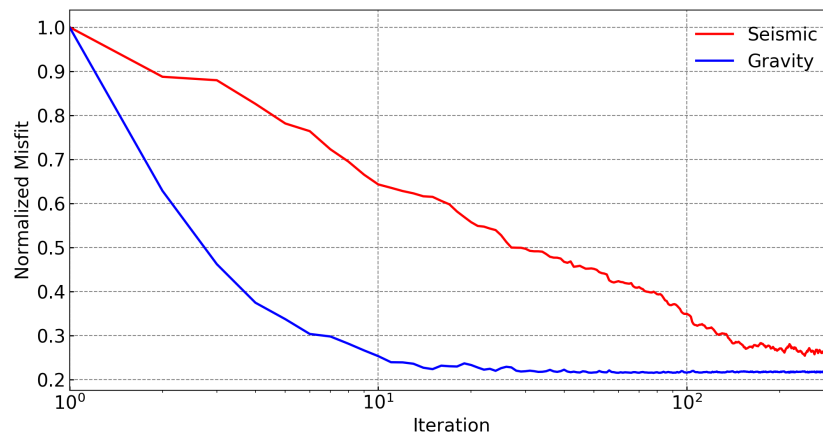
For this example we created a 3D model based on the structure of the Texas-shape model I and discretize it with a mesh of size: $n_x = 50, n_y = 50$ and $n_z = 25$. The model consists of 4 primary structures of high velocity (Fig. 7a) surrounded by low-velocity layers, constant along the y -direction (7e). The central structure is a 3D Texas-shaped body (Fig. 7b), primarily concentrated at $y = 1120$ m with a velocity of 3050 m/s. There are two other structures located approximately in the x - z plane for $y = 1800$ m with velocities of 2500 and 2800 m/s respectively, as shown in Fig. 7c. Finally, a fourth object is centered at $y = 200$ m with a velocity of 2900 m/s with the shape of a banana. The density model for this example (not shown) is obtained from Gardner's equation. The inversion and modelling parameter for this model are similar to the previous examples, however, we have increased the number of sources to $n_s = n_{s_x} \times n_{s_y} = 10 \times 10 = 100$ and the number of receivers to $n_r = n_{r_x} \times n_{r_y} = 50 \times 50 = 2500$ equally spaced along the surface and we use a peak frequency of 8 Hz given the grid used. We perform 100 iterations of the cooperative inversion scheme using the 3D starting model shown in Fig. 7f.



(a)



(b)



(c)

Fig. 6. (a) Comparison of observed (black), initial synthetic (red) and final synthetic traces measured at 300 m due to a source applied at 200 m on the surface for the Texas-shaped model II. The observed data was contaminated with noise. (b) Normalized true (black dots), starting (red line) and final (blue line) gravimetric responses result for the Texas-shaped model II adding noise to the data. (c) Normalized misfit for seismic (red) and gravity (blue) for the Texas-shaped model II.

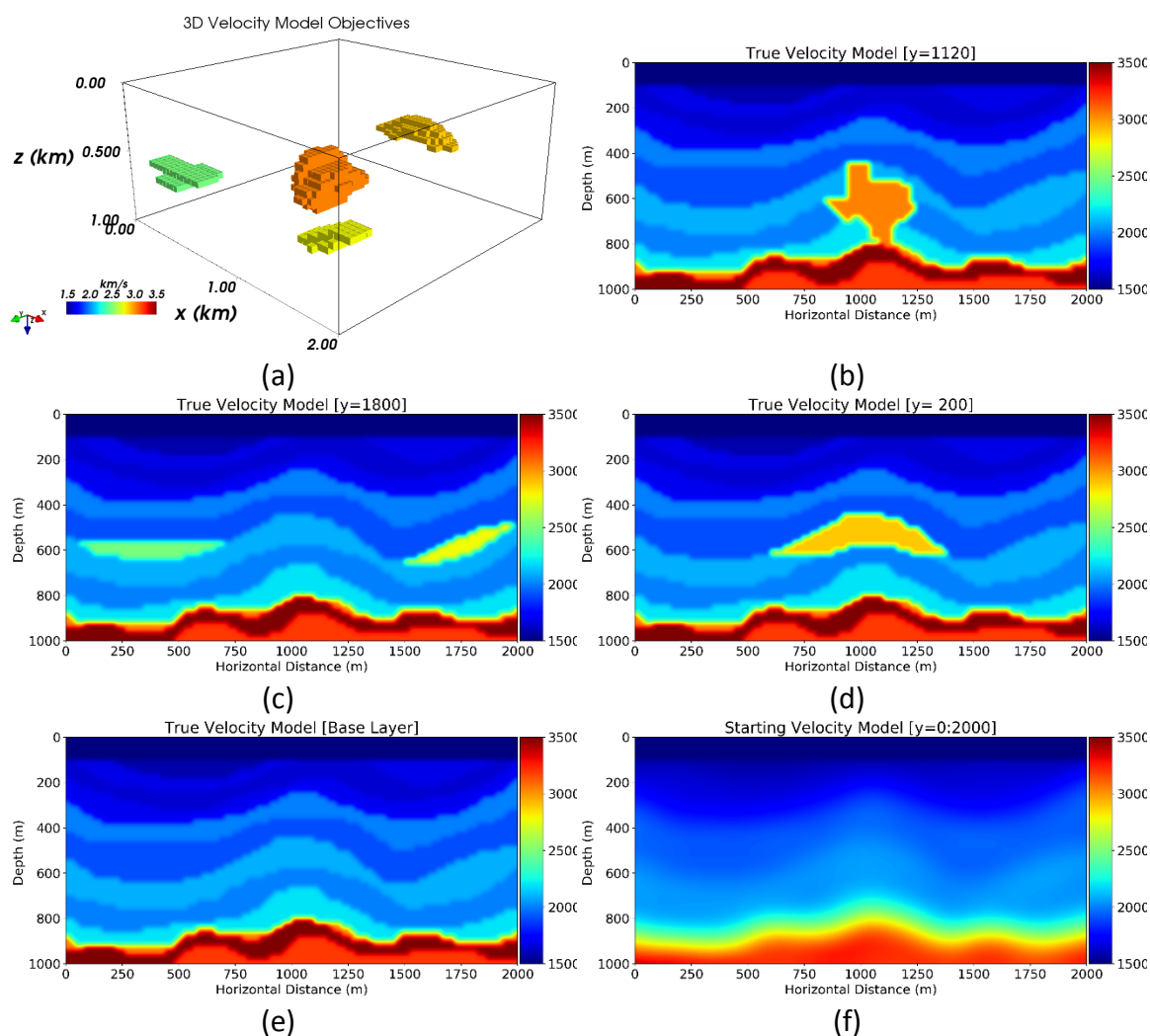


Fig. 7. 3D velocity model for cooperative inversion, where (a) shows the four objectives and (b), (c) and (d) 2D views at constant y . (e) The layered model in the x - z plane (it is constant in the y -direction). (f) The starting model is a smooth version of the layered model.

Similar to the previous 2D results, the method successfully recovers the main features of the model (Fig. 8). The shape and position of the main object are recovered, nevertheless, the total mass is not fully recovered (compare Figs. 8c and 8d). The other 3 bodies and the layered structure are also recovered, as shown in Figs. 8b and 8f.

The data misfits (Fig. 9) show a relatively fast convergence for the seismic data. The gravimetric misfit shows an increase in the first part because the method gives more weight to FWI, however, it exhibits good convergence after the 6th iteration. In the later iterations the seismic misfit starts showing a slow convergence whereas the gravimetric misfit shows further improvement. The slow convergence of FWI is due to the moderate

accretion of velocity and density in the Texas-shaped body and the other structures.

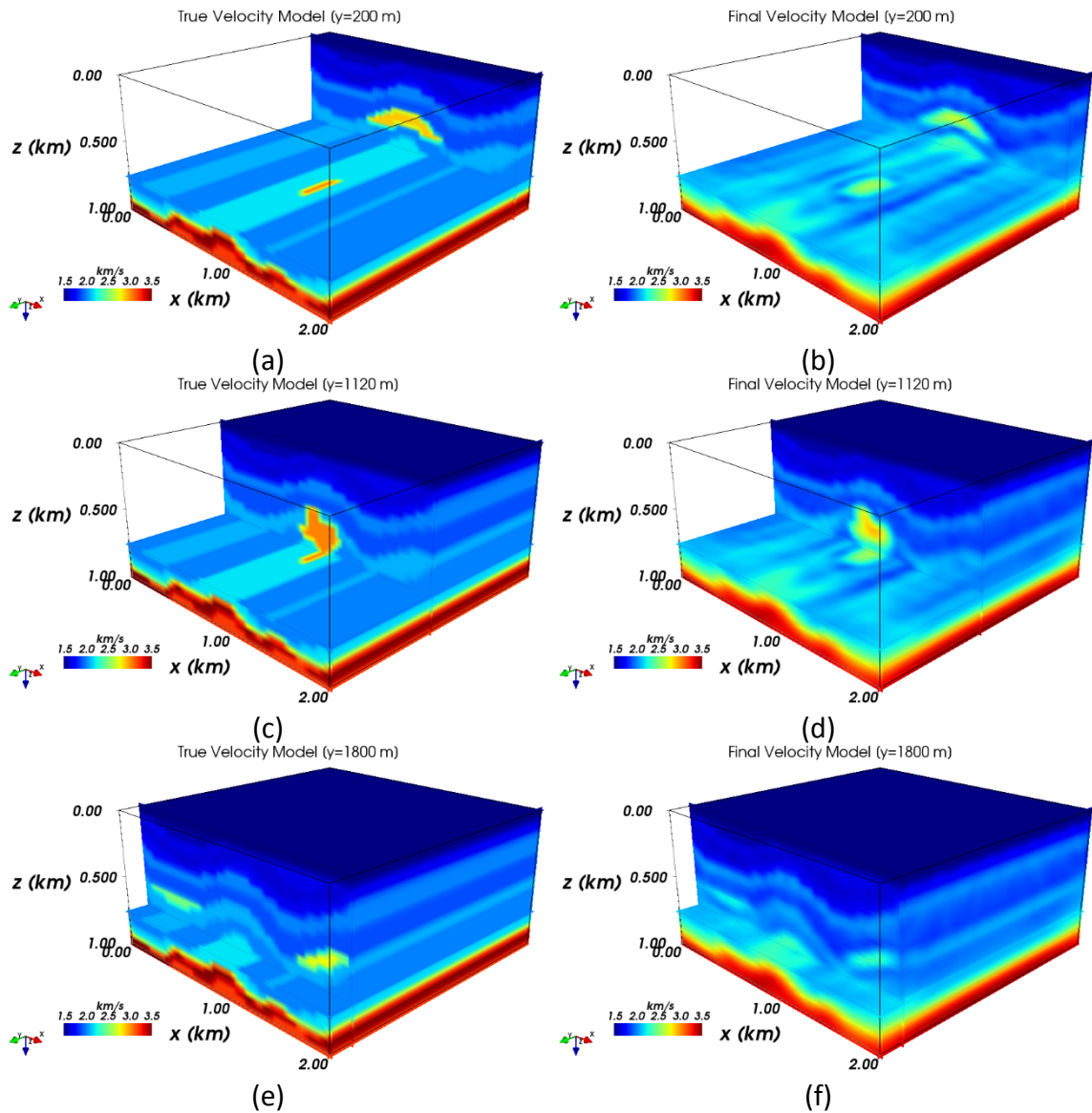


Fig. 8. 3D velocity models for different y-views for the true model (left) and the cooperative inversion results (right).

The starting and final gravity residual are shown in Figs. 10a and 10b respectively. The starting residual is mainly due to the Texas-shape body. Besides that, the other objectives also contribute to the residual in their respective regions. The final gravimetric residual has been normalized with respect to the starting residual, the contour of the starting residual is displayed in Fig. 10b facilitate the comparison. Notice that the amplitude of the residual has been reduced one order of magnitude.

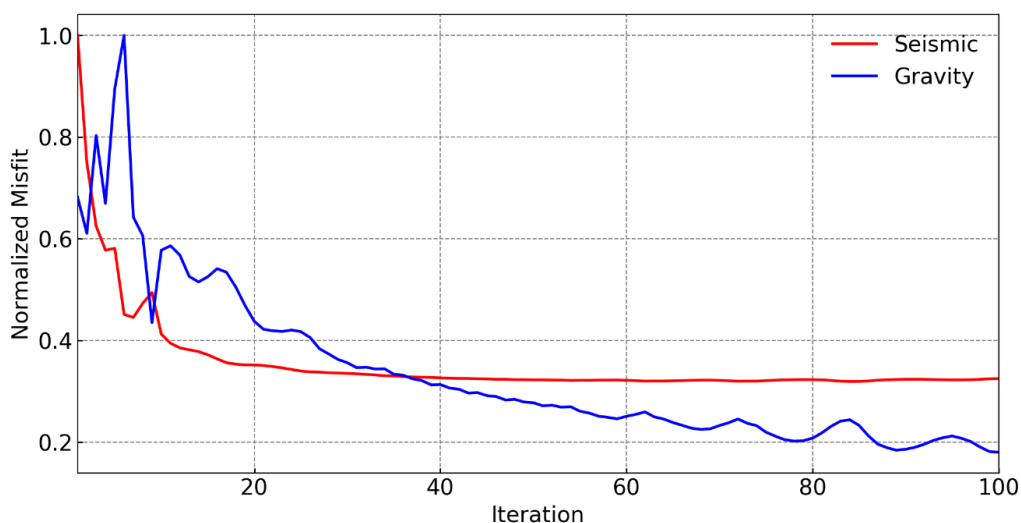


Fig. 9. Normalized misfit for seismic (red) and gravity (blue) for the 3D example.

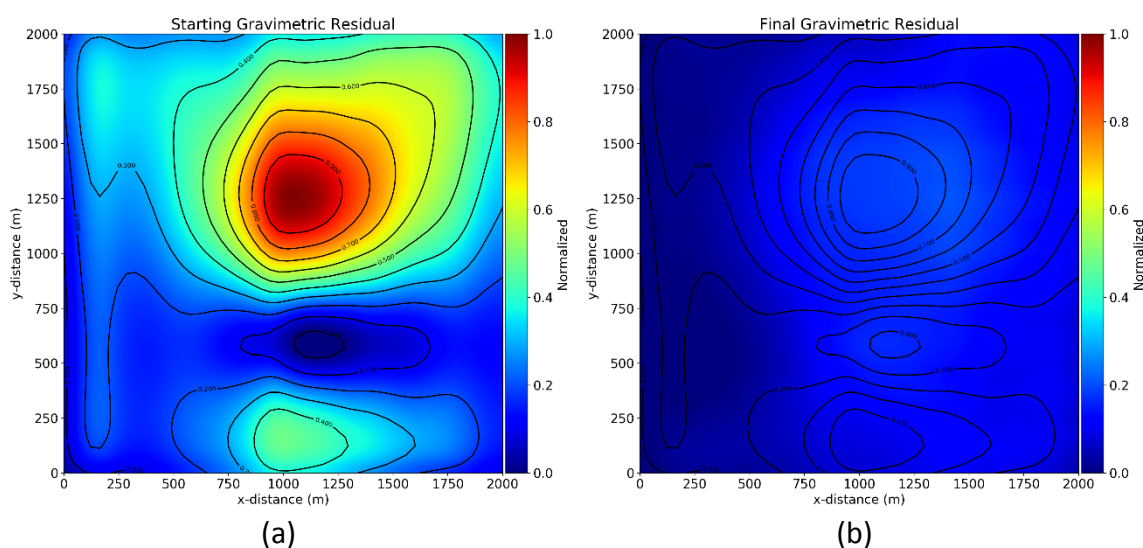


Fig. 10. Starting gravimetric residual (a) and final gravimetric residual (b) after cooperative inversion. Both residuals are normalized with respect to the starting residual and the starting contours are displayed in the final to illustrate the regions where the residual is reduced.

In order to compare the fit of the seismic data, we select three receivers with different source position and show the observed (black dashed), starting (red) and final (blue) pressures seismograms in Fig. 11. The three seismograms are strategically located near the different velocity objectives (Fig. 7a) as show in Table 2. Consistently with the convergence of the seismic misfit (Fig. 9), the seismograms from the final iteration match

the observed pressure for all receivers as shown in Fig. 11. All the events are matched with only minor discrepancies. Therefore, we conclude that both geophysical data sets are fitted with proper 3D velocity and density models.

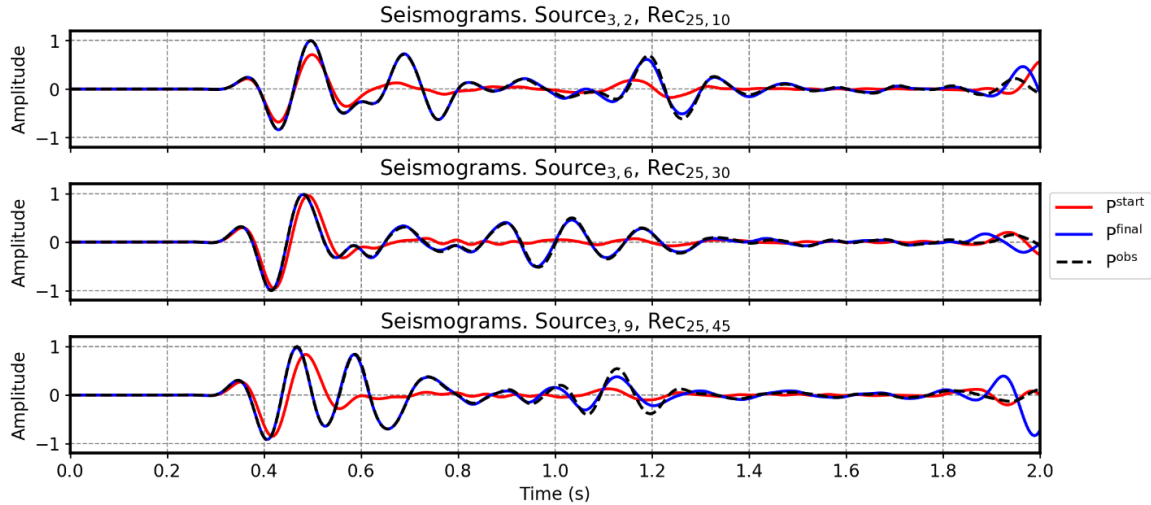


Fig. 11. Seismic data fit for different sources and receivers for observed pressure (black dashed), starting synthetic pressure (red) and final synthetic pressure (blue) after 100 iterations of cooperative inversion.

Table 2. Source and receiver position for the three seismograms selected to compare the data fit.

| Source Position (x, y) [m] | Receiver Position (x, y) [m] | Nearest Velocity Target |
|-----------------------------------|-------------------------------------|----------------------------|
| (444.44, 222.22) | (1020.41, 408.16) | Figure 23d |
| (444.44, 1111.11) | (1020.41, 1224.49) | Figure 23b |
| (444.44, 1777.78) | (1020.41, 1836.73) | Figure 23c |

CONCLUSIONS

Gravimetric and Full Waveform Inversion in a cooperative scheme based on petrophysical relationships can be used to characterize irregular high velocity-density bodies embedded in a complex geology. As long as the starting model is acceptable and FWI has more weight in the cooperative inversion algorithm, both methods converge recovering, for the three synthetic models presented, the stratigraphic part and the top and shape of the deepest body.

We have compared through numerical examples the proposed approach with conventional FWI and joint inversion. The computational cost of the cooperative approach is similar to that of FWI and significantly smaller than that of conventional joint inversion. The main reason for the differences in compute times is that the joint inversion requires computing the Fréchet derivatives, whereas FWI and the cooperative approach can be more efficiently implemented using the adjoint method. On the other hand, the cooperative approach successfully incorporates seismic and gravimetric data, yielding a unified model that profits from both geophysical methods.

Another important aspect of our proposed scheme is the use of the same grid structure in gravity and FWI. These results are promising and encourage us to apply the proposed cooperative scheme to the elastic case. We have used Gardner's petrophysical relations, however, these are not applicable to some lithologies of interest in exploration seismology.

ACKNOWLEDGEMENTS

We would like to express our gratitude to CONACYT (Mexican National Council for Science and Technology) for the scholarship granted to Raul Ulices Silva Avalos. The numerical computations for this work were performed using the cluster Lamb of the supercomputing lab at the Specialized Labs System of the Earth Sciences Division of CICESE. Part of this work was developed during a research visit at the Institute for Geophysics of The University of Texas at Austin.

REFERENCES

- Alford, R., Kelly, K. and Boore, D.M., 1974. Accuracy of finite-difference modeling of the acoustic wave equation. *Geophysics*, 39: 834-842.
- Banerjee, B. and Das Gupta, S., 1977. Gravitational attraction of a rectangular parallelepiped. *Geophysics*, 42: 1053-1055.
- Bhattacharyya, B. and Leu, L.-K., 1977. Spectral analysis of gravity and magnetic anomalies due to rectangular prismatic bodies. *Geophysics*, 42: 41-50.
- Blakely, R.J., 1996. *Potential Theory in Gravity and Magnetic Applications*. Cambridge University Press, Cambridge.
- Blom, N., Boehm, C. and Fichtner, A., 2017. Synthetic inversions for density using seismic and gravity data. *Geophys. J. Internat.*, 209: 1204-1220.
- Boulanger, O. and Chouteau, M., 2001. Constraints in 3D gravity inversion. *Geophys. Prosp.*, 49: 265-280.
- Brocher, T.M., 2005. Empirical relations between elastic wavespeeds and density in the Earth's crust. *Bull. Seismol. Soc. Am.*, 95: 2081-2092.
- Cohen, G., 2002. *Higher-order Numerical Methods for Transient Wave Equations*. Springer Verlag, Berlin.
- Colombo, D. and Rovetta, D., 2018. Coupling strategies in multiparameter geophysical joint inversion. *Geophys. J. Internat.*, 215: 1171-1184.

- Gallardo, L.A. and Meju, M.A., 2003. Characterization of heterogeneous near-surface materials by joint 2D inversion of DC resistivity and seismic data. *Geophys. Res. Lett.*, 30: 13.
- Gallardo, L.A. and Meju, M.A., 2004. Joint two-dimensional DC resistivity and seismic travel time inversion with cross-gradients constraints. *J. Geophys. Res., Solid Earth*, (1978-2012), 109(B3).
- García-Abdeslem, J., 2005. The gravitational attraction of a right rectangular prism with density varying with depth following a cubic polynomial. *Geophysics*, 70(6): J39-J42.
- Gardner, G., Gardner, L. and Gregory, A., 1974. Formation velocity and density - The diagnostic basics for stratigraphic traps. *Geophysics*, 39: 770-780.
- Hansen, P.C., 1992. Analysis of discrete ill-posed problems by means of the L-curve. *SIAM review*, 34: 561-580.
- Johnson, L.R. and Litehiser, J.J., 1972. A method for computing the gravitational attraction of three-dimensional bodies in a spherical or ellipsoidal Earth. *J. Geophys. Res.*, 77: 6999-7009.
- Komatitsch, D. and Tromp, J., 1999. Introduction to the spectral element method for three-dimensional seismic wave propagation. *Geophys. J. Internat.*, 139: 806-822.
- Lees, J.M. and Van Decar, J., 1991. Seismic tomography constrained by Bouguer gravity anomalies: Applications in western Washington. *Pure Appl. Geophys.*, 135: 31-52.
- Lin, F.-C., Schmandt, B. and Tsai, V.C., 2012. Joint inversion of Rayleigh wave phase velocity and ellipticity using USArray: Constraining velocity and density structure in the upper crust. *Geophys. Res. Lett.*, 39: (12).
- Lin, W. and Zhdanov, M., 2017. Joint inversion of seismic and gravity gradiometry data using Gramian constraints. *Expanded Abstr.*, 87th Ann. Internat. SEG Mtg., Houston: 1734-1738.
- Li, Y. and Oldenburg, D.W., 1998. 3-D inversion of gravity data. *Geophysics*, 63: 109-119.
- Marfurt, K.J., 1984. Accuracy of finite-difference and finite-element modeling of the scalar and elastic wave equations. *Geophysics*, 49: 533-549.
- Martin, R., Chevrot, S., Komatitsch, D., Seoane, L., Spangenberg, H., Wang, Y., Dufrechou, G., Bonvalot, S. and Bruinsma, S., 2017. A high-order 3-D spectral-element method for the forward modelling and inversion of gravimetric data - Application to the western Pyrenees. *Geophys. J. Internat.*, 209: 406-424.
- Menichetti, V. and Guillen, A., 1983. Simultaneous interactive magnetic and gravity inversion. *Geophys. Prosp.*, 31: 929-944.
- Nagy, D., 1966. The gravitational attraction of a right rectangular prism. *Geophysics*, 31: 362-371.
- Paasche, H. and Tronicke, J., 2007. Cooperative inversion of 2D geophysical data sets: A zonal approach based on fuzzy c-means cluster analysis. *Geophysics*, 72(3): A35-A39.
- Plessix, R.-E., 2006. A review of the adjoint-state method for computing the gradient of a functional with geophysical applications. *Geophys. J. Internat.*, 167: 495-503.
- Romero, A. and Gallardo, L.A., 2015. Borehole constrained inversion of geophysical data based on fuzzy clustering. *Expanded Abstr.*, 85th Ann. Internat. SEG Mtg., New Orleans: 1792-1796.
- Roy, L., Sen, M.K., McIntosh, K., Stoffa, P.L. and Nakamura, Y., 2005. Joint inversion of first arrival seismic travel-time and gravity data. *J. Geophys. Engineer.*, 2: 277.
- Sen, M.K. and Stoffa, P.L., 2013. *Global Optimization Methods in Geophysical Inversion*. Cambridge University Press, Cambridge
- Sheriff, R.E. and Geldart, L.P., 1995. *Exploration Seismology*. Cambridge University Press, Cambridge.

- Talwani, M., 1965. Computation with the help of a digital computer of magnetic anomalies caused by bodies of arbitrary shape. *Geophysics*, 30: 797-817.
- Tarantola, A., 1984. Inversion of seismic reflection data in the acoustic approximation. *Geophysics*, 49: 1259-1266.
- Tarantola, A., 1986. A strategy for nonlinear elastic inversion of seismic reflection data. *Geophysics*, 51: 1893-1903.
- Tondi, R., Achauer, U., Landes, M., Daví, R. and Besutiu, L., 2009. Unveiling seismic and density structure beneath the Vrancea seismogenic zone, Romania. *J. Geophys. Res.: Solid Earth*, 114: B11.
- Vigh, D. and Starr, E.W., 2008. 3D prestack plane-wave, full-waveform inversion. *Geophysics*, 73(5). VE135-VE144.
- Virieux, J., 1986. P-SV wave propagation in heterogeneous media: Velocity-stress finite-difference method. *Geophysics*, 51: 889-901.
- Virieux, J. and Operto, S., 2009. An overview of full-waveform inversion in exploration geophysics. *Geophysics*, 74(6): WCC1-WCC26.
- Vozoff, K. and Jupp, D., 1975. Joint inversion of geophysical data. *Geophys. J. Internat.*, 42: 977-991.
- Werner, R.A., 1994. The gravitational potential of a homogeneous polyhedron or don't cut corners. *Celest. Mech. Dynamic. Astron.*, 59: 253-278.
- Zeyen, H. and Pous, J., 1993. 3-D joint inversion of magnetic and gravimetric data with a-priori information. *Geophys. J. Internat.*, 112: 244-256.
- Zhdanov, M.S., Ellis, R. and Mukherjee, S., 2004. Three-dimensional regularized focusing inversion of gravity gradient tensor component data. *Geophysics*, 69: 925-937.